
BiSSL: A Bilevel Optimization Framework for Enhancing the Alignment Between Self-Supervised Pre-Training and Downstream Fine-Tuning

Gustav Wagner Zakarias^{1,2} Lars Kai Hansen^{3,2} Zheng-Hua Tan^{1,2}

Abstract

This study presents BiSSL, a novel training framework that utilizes bilevel optimization to enhance the alignment between the pretext pre-training and downstream fine-tuning stages in self-supervised learning. BiSSL formulates the pretext and downstream task objectives as the lower- and upper-level objectives in a bilevel optimization problem and serves as an intermediate training stage within the self-supervised learning pipeline. By explicitly modeling the interdependence of these training stages, BiSSL facilitates enhanced information sharing between them, ultimately leading to a backbone parameter initialization that is better aligned for the downstream task. We propose a versatile training algorithm that alternates between optimizing the two objectives defined in BiSSL, which is applicable to a broad range of pretext and downstream tasks. Using SimCLR and Bootstrap Your Own Latent to pre-train ResNet-50 backbones on the ImageNet dataset, we demonstrate that our proposed framework significantly outperforms the conventional self-supervised learning pipeline on the vast majority of 12 downstream image classification datasets, as well as on object detection. Visualizations of the backbone features provide further evidence that BiSSL improves the downstream task alignment of the backbone features prior to fine-tuning.

tions are learned by solving a pretext task, which operates on supervisory signals extracted from the unlabeled data itself. Extensive efforts have been dedicated to designing effective pretext tasks, leading to state-of-the-art or competitive performance in various fields such as computer vision (Chen et al., 2020b; Bardes et al., 2022; He et al., 2020; Grill et al., 2020; Caron et al., 2020; 2021; He et al., 2022; Oquab et al., 2024), natural language processing (Devlin et al., 2019; Lewis et al., 2019; Brown et al., 2020; He et al., 2021; Touvron et al., 2023) and audio signal processing (Schneider et al., 2019; Baevski et al., 2020; Hsu et al., 2021; Niizumi et al., 2021; Chung & Glass, 2018; Chung et al., 2019; Yadav et al., 2024). A key advantage of SSL is that it enables the reuse of pre-trained model backbones, eliminating the need to train models from scratch and thereby facilitating efficient adaptation to specific downstream tasks.

Making a self-supervised pre-trained model backbone suitable for a downstream task typically involves attaching additional layers that are compatible with that task, followed by fine-tuning the entire or parts of the composite model in a supervised manner (Zhai et al., 2019; Dubois et al., 2022). When a backbone is pre-trained on a distribution that differs from the distribution of the downstream data, the representations learned during pre-training may not be initially well-aligned with the downstream task. During fine-tuning, this distribution misalignment could cause relevant semantic information, learned during the pre-training phase, to vanish from the representation space (Zaiem et al., 2024; Chen et al., 2020a; Boschini et al., 2022). A potential strategy for alleviating the negative effects of these distribution discrepancies would be to enhance the alignment between the pretext pre-training and downstream fine-tuning stages. However, since the conventional SSL pipeline treats these stages as two disjoint processes, this poses a significant challenge in devising a strategy that enhances such alignment while not compromising on the benefits that SSL offers.

Meanwhile, bilevel optimization (BLO) has risen as a powerful tool for solving certain optimization problems within deep learning. It entails a main optimization problem constrained by the solution to a secondary optimization problem that depends on the parameters of the main optimization objective. This hierarchical setup causes the solutions of

1. Introduction

In the absence of sufficient labeled data, self-supervised learning (SSL) provides a powerful framework for training deep learning models. SSL leverages large amounts of unlabeled data to learn representations that can be effectively utilized across various downstream tasks. These representa-

¹Aalborg University ²Technical University of Denmark
³Pioneer Centre for Artificial Intelligence, Denmark. Correspondence to: Gustav Wagner Zakarias <gwz@es.aau.dk>, Zheng-Hua Tan <zt@es.aau.dk>.

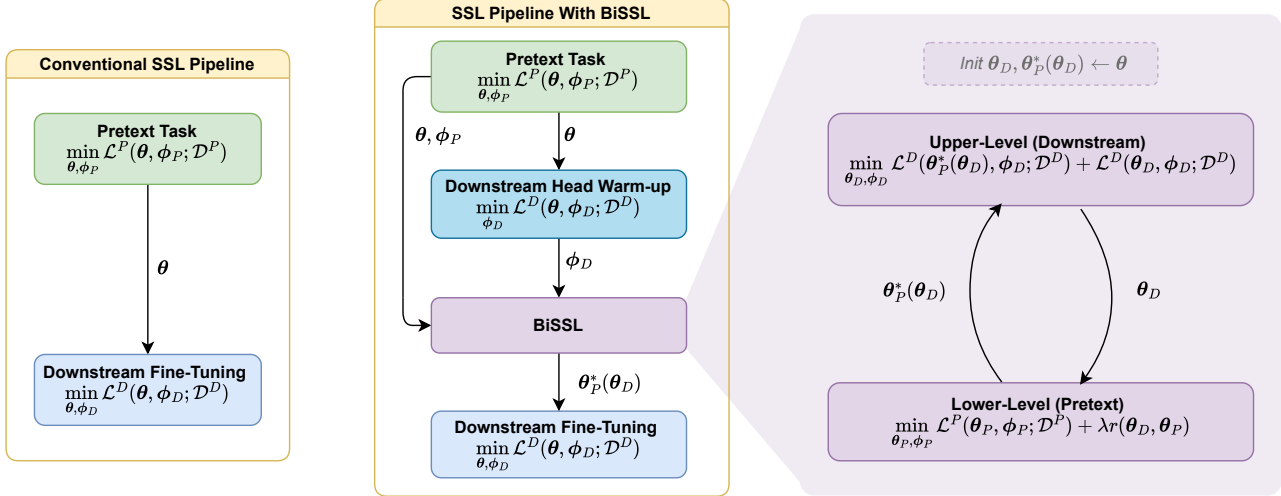


Figure 1. The conventional self-supervised learning pipeline alongside the proposed pipeline involving BiSSL. The symbols θ and ϕ represent obtained backbone and task-specific attached head parameters, respectively. When they are transmitted to the respective training stages, they are used as initializations.

both optimization problems to depend on each other, either directly or implicitly, which has proven advantageous in deep learning tasks that optimize multiple inter-dependent objectives simultaneously (Zhang et al., 2023a). Notable mentions of tasks within deep learning where BLO has proven useful are parameter pruning (Zhang et al., 2022b), invariant risk minimization (Arjovsky et al., 2019; Zhang et al., 2023b), meta-learning (Rajeswaran et al., 2019; Finn et al., 2017), adversarial robustness (Zhang et al., 2021), hyper-parameter optimization (Franceschi et al., 2018) and coreset selection (Borsos et al., 2020).

In this study, we propose BiSSL, a novel training framework that leverages BLO to enhance the alignment between the pretext pre-training and downstream fine-tuning stages in SSL. Acting as an intermediate training stage within the SSL pipeline, BiSSL frames the pretext and downstream task objectives as the lower- and upper-level objectives in a BLO problem. The objectives in BiSSL are connected by substituting the lower-level backbone solution for the upper-level backbone parameters, while simultaneously enforcing the lower-level backbone solution to resemble the upper-level backbone parameters. This approach more explicitly captures the interdependence between pretext pre-training and downstream fine-tuning, fostering a lower-level backbone that is better aligned with the downstream task. Figure 1 compares the conventional SSL pipeline with our suggested training pipeline involving BiSSL. Additionally, we introduce a training algorithm that alternates between optimizing the two objectives within BiSSL, which is agnostic to the choice of pretext and downstream task. Through

experiments using both the SimCLR (Chen et al., 2020b) and Bootstrap Your Own Latent (BYOL) Grill et al. (2020) pretext tasks to pre-train ResNet-50 backbones (He et al., 2016) on the ImageNet-1K dataset (Deng et al., 2009), we demonstrate that BiSSL significantly improves downstream performance across most of 12 downstream image classification datasets, while also excelling in object detection. The code implementation and pre-trained model weights are publicly available.¹

2. Related Work

Bilevel Optimization in Self-Supervised Learning

Bilevel optimization (BLO) refers to a constrained optimization problem, where the constraint itself is a solution to another optimization problem which depends on the parameters of the “main” optimization problem. The general BLO problem is formulated as

$$\min_{\xi} f(\xi, \psi^*(\xi)) \quad \text{s.t.} \quad \psi^*(\xi) \in \underset{\psi}{\operatorname{argmin}} g(\xi, \psi), \quad (1)$$

where f and g are referred to as the upper-level and lower-level objectives, respectively. While the lower objective g has knowledge of the parameters ξ from the upper-level objective, the upper-level objective f possesses full information of the lower objective g itself through its dependence on the lower-level solution $\psi^*(\xi)$. Some works have incorporated bilevel optimization within self-supervised learning. Gupta et al. (2022) suggest formulating the contrastive self-

¹https://github.com/ICML25-10807/ICML25_10807_BiSSL

supervised pretext task as a bilevel optimization problem, dedicating the upper-level and lower-level objectives for updating the backbone and projection head parameters respectively. Other frameworks such as the Local and Global (LoGo) (Zhang et al., 2022a) and Only Self-Supervised Learning (OSSL) Boonlia et al. (2022) utilize auxiliary models, wherein the lower-level objective optimizes the parameters of the auxiliary model, while the upper-level objective is dedicated to training the feature extraction model. MetaMask (Li et al., 2022b) introduces a meta-learning based approach, where the upper-level learns masks that filter out irrelevant information from inputs that are provided to a lower-level self-supervised contrastive pretext task. BLO-SAM (Zhang et al., 2024) is tailored towards fine-tuning the segment anything model (SAM) (Kirillov et al., 2023) by interchangeably alternating between learning (upper-level) prompt embeddings and fine-tuning the (lower-level) segmentation model. The aforementioned frameworks integrate bilevel optimization into *either* the pre-training or fine-tuning stage exclusively and are tailored towards specific pretext or downstream tasks. In contrast, our proposed BiSSL employs a BLO problem that comprehensively incorporates *both* training stages of pretext pre-training and downstream fine-tuning, while not being confined to any specific type of pretext or downstream task.

Priming Pre-Trained Backbones Prior To Fine-Tuning

Previous works have demonstrated that downstream performance can be enhanced by introducing techniques that modify the backbone between the pre-training and fine-tuning stages. Contrastive Initialization (COIN) (Pan et al., 2022) introduces a supervised contrastive loss to be utilized on backbones pre-trained with contrastive SSL techniques. Noisy-Tune (Wu et al., 2022) perturbs the pre-trained backbone with tailored noise before fine-tuning. Speaker-invariant clustering (Spin) (Chang et al., 2023) utilizes speaker disentanglement and vector quantization for improving speech representations for speech signal specific downstream tasks. RIFLE (Li et al., 2020) conducts multiple fine-tuning sessions sequentially, where the attached downstream specific layers are re-initialized in between every session. Unlike BiSSL, these techniques either do not incorporate knowledge of both the pretext task and downstream task objectives and their relationship, or do so only implicitly.

3. Proposed Method

3.1. Notation

We denote the unlabeled pretext dataset $\mathcal{D}^P = \{\mathbf{z}_k\}_{k=1}^{C_P}$ and labeled downstream dataset $\mathcal{D}^D = \{\mathbf{x}_l, \mathbf{y}_l\}_{k=1}^{C_D}$, respectively, where $\mathbf{z}_k, \mathbf{x}_l \in \mathbb{R}^N$. Let $f_\theta : \mathbb{R}^N \rightarrow \mathbb{R}^M$ denote a feature extracting backbone with trainable parameters θ and

$h_\phi^T : \mathbb{R}^M \rightarrow \mathbb{R}^{Q_T}$ a task specific head with trainable parameters ϕ . Given pretext and downstream models $h_{\phi_P}^P \circ f_{\theta_P}$ and $h_{\phi_D}^D \circ f_{\theta_D}$ with $\theta_P, \theta_D \in \mathbb{R}^L$, we denote the pretext and downstream training objectives $\mathcal{L}^P(\theta_P, \phi_P; \mathcal{D}^P)$ and $\mathcal{L}^D(\theta_D, \phi_D; \mathcal{D}^D)$, respectively. To simplify notation, we omit the dataset specification from the training objectives, e.g. $\mathcal{L}^D(\theta_D, \phi_D) := \mathcal{L}^D(\theta_D, \phi_D; \mathcal{D}^D)$.

3.2. Optimization Problem Formulation

The conventional setup of self-supervised pre-training directly followed by supervised fine-tuning relies on using a single backbone model with parameters θ . In that instance, we minimize $\mathcal{L}^P(\theta_P, \phi_P)$ to produce a backbone parameter configuration θ_P^* which is then used as an initialization when subsequently minimizing the downstream training objective $\mathcal{L}^D(\theta_D, \phi_D)$. We deviate from this by instead considering θ_P and θ_D as two separate parameter vectors that are strongly correlated. In continuation, we suggest combining the two traditionally separate optimization problems of pretext and downstream training into a joint optimization problem through bilevel optimization, that we term BiSSL. We formulate BiSSL as

$$\begin{aligned} \min_{\theta_D, \phi_D} \mathcal{L}^D(\theta_P^*(\theta_D), \phi_D) + \mathcal{L}^D(\theta_D, \phi_D) \quad (2) \\ \text{s.t. } \theta_P^*(\theta_D) \in \underset{\theta_P}{\operatorname{argmin}} \min_{\phi_P} \mathcal{L}^P(\theta_P, \phi_P) + \lambda r(\theta_D, \theta_P), \quad (3) \end{aligned}$$

with r being some convex regularization objective weighted by $\lambda \in \mathbb{R}_+$ enforcing similarity between θ_D and θ_P . The upper-level training objective in (2) is tasked with minimizing the downstream task objective \mathcal{L}^D , while the lower-level objective in (3) aims to minimize the pretext task objective \mathcal{L}^P while also ensuring its backbone remains similar to the upper-level backbone. As seen in the left term of (2), the backbone parameters $\theta_P^*(\theta_D)$ are transferred into the downstream training objective, mirroring how the backbone is transferred in the conventional SSL pipeline. Although the second term of (2) is not strictly necessary, it has empirically shown to improve stability and aid convergence of the upper-level solution during training. Unlike the traditional SSL setup, the backbone solution of the pretext objective $\theta_P^*(\theta_D)$ is now a function of the parameters of the downstream backbone θ_D , since the lower-level problem is dependent on the upper-level backbone parameters.

As the upper-level objective in (2) depends on the solution $\theta_P^*(\theta_D)$ of the lower-level problem in (3), this enables the incorporation of information from the pretext objective when solving the upper-level optimization problem. By including a regularization objective r that enforces similarity between the lower-level and upper-level backbone parameters, this setup is expected to guide the lower-level optimization toward a configuration of model backbone pa-

rameters that is more beneficial for subsequent fine-tuning on the downstream task. To more specifically understand how the pretext objective influences the downstream training procedure in this setup, we delve deeper into the gradient expression of the upper-level training objective in (2) in the following subsection.

3.3. Upper-level Derivative

Given the upper-level objective $F(\boldsymbol{\theta}_D, \phi_D) := \mathcal{L}^D(\boldsymbol{\theta}_P^*(\boldsymbol{\theta}_D), \phi_D) + \mathcal{L}^D(\boldsymbol{\theta}_D, \phi_D)$ from (2), its derivative with respect to $\boldsymbol{\theta}_D$ is given by

$$\frac{dF}{d\boldsymbol{\theta}_D} = \underbrace{\frac{d\boldsymbol{\theta}_P^*(\boldsymbol{\theta}_D)^T}{d\boldsymbol{\theta}_D}}_{\text{IG}} \nabla_{\boldsymbol{\theta}} \mathcal{L}^D(\boldsymbol{\theta}, \phi_D)|_{\boldsymbol{\theta}=\boldsymbol{\theta}_P^*(\boldsymbol{\theta}_D)} + \nabla_{\boldsymbol{\theta}} \mathcal{L}^D(\boldsymbol{\theta}, \phi_D)|_{\boldsymbol{\theta}=\boldsymbol{\theta}_D}. \quad (4)$$

Due to the dependence of the lower-level solution on the upper-level parameters, the first term of (4) includes the implicit gradient (IG) of the implicit function $\boldsymbol{\theta}_P^*(\boldsymbol{\theta}_D)$. To simplify notation, we let $\nabla_{\boldsymbol{\xi}} h(\boldsymbol{\xi})|_{\boldsymbol{\xi}=\boldsymbol{\psi}} := \nabla_{\boldsymbol{\xi}} h(\boldsymbol{\psi})$ when it is clear from context which variables are differentiated with respect to. Following an approach similar to Rajeswaran et al. (2019), with details on the derivations and underlying assumptions outlined in Section A.1 of Appendix A, the IG in (4) can be explicitly expressed as

$$\frac{d\boldsymbol{\theta}_P^*(\boldsymbol{\theta}_D)^T}{d\boldsymbol{\theta}_D} = -\nabla_{\boldsymbol{\theta}_D \boldsymbol{\theta}_P}^2 r(\boldsymbol{\theta}_D, \boldsymbol{\theta}_P^*(\boldsymbol{\theta}_D)) \cdot \left[\nabla_{\boldsymbol{\theta}}^2 \left(\frac{1}{\lambda} \mathcal{L}^P(\boldsymbol{\theta}_P^*(\boldsymbol{\theta}_D), \phi_P) + r(\boldsymbol{\theta}_D, \boldsymbol{\theta}_P^*(\boldsymbol{\theta}_D)) \right) \right]^{-1}, \quad (5)$$

A common convex regularization objective, which will also be the choice in the subsequent experiments of this work, is $r(\boldsymbol{\xi}, \boldsymbol{\psi}) = \frac{1}{2} \|\boldsymbol{\xi} - \boldsymbol{\psi}\|_2^2$. Using this regularization objective simplifies (5) down to

$$\frac{d\boldsymbol{\theta}_P^*(\boldsymbol{\theta}_D)^T}{d\boldsymbol{\theta}_D} = \left[\frac{1}{\lambda} \nabla_{\boldsymbol{\theta}}^2 \mathcal{L}^P(\boldsymbol{\theta}_P^*(\boldsymbol{\theta}_D), \phi_P) + I_L \right]^{-1}, \quad (6)$$

where I_L is the $L \times L$ -dimensional identity matrix. Hence the upper-level derivative in (4) can be expressed as

$$\frac{dF}{d\boldsymbol{\theta}_D} = \left[\frac{1}{\lambda} \nabla_{\boldsymbol{\theta}}^2 \mathcal{L}^P(\boldsymbol{\theta}_P^*(\boldsymbol{\theta}_D), \phi_P) + I_L \right]^{-1} \cdot \nabla_{\boldsymbol{\theta}} \mathcal{L}^D(\boldsymbol{\theta}_P^*(\boldsymbol{\theta}_D), \phi_D) + \nabla_{\boldsymbol{\theta}} \mathcal{L}^D(\boldsymbol{\theta}_D, \phi_D). \quad (7)$$

The inverse Hessian-vector product in (7) is computationally infeasible to calculate directly, so it is approximated using the conjugate gradient (CG) method (Nazareth, 2009; Shewchuk, 1994). We employ a layer-wise implementation of the CG method based on that of Rajeswaran et al. (2019) and refer to their work for more details on applying CG in a

deep learning setup with BLO. While CG has proven to be an effective approach for approximating the inverse Hessian-vector products in previous works (Pedregosa, 2016; Zhang et al., 2021; Rajeswaran et al., 2019), it still introduces some computational overhead due to its need for evaluations of multiple Hessian vector products. Future work could explore alternative established methods for upper-level gradient approximation (Zhang et al., 2023a; Choe et al., 2023; Lorraine et al., 2020) that offer greater computational efficiency without compromising downstream task performance.

With an explicit expression of the IG in (6), we can interpret the impact of the scaling factor λ from (3) and (7): When λ is very large, the dependence of the lower-level objective on the upper-level parameters $\boldsymbol{\theta}_D$ is also very large. This effectively drives the lower-level backbone parameters toward the trivial solution $\boldsymbol{\theta}_P^*(\boldsymbol{\theta}_D) = \boldsymbol{\theta}_D$. Meanwhile, the IG in (6) approximately equals I_L , thereby diminishing the influence of the lower-level objective on the upper-level gradient in (7). This roughly makes the task of the upper-level equivalent to conventional fine-tuning. Conversely, if λ is very small, the lower-level objective in (3) effectively defaults to conventional pretext task training. Additionally, the implicit gradient in (6) would consist of numerically tiny entries, making the optimization of the first term in the upper-level objective in (2) equivalent to probing of the downstream head on the frozen pretext backbone $\boldsymbol{\theta}_P^*(\boldsymbol{\theta}_D)$.

3.4. Training Algorithm and Pipeline

Algorithm 1 outlines the proposed training algorithm, which iteratively alternates between solving the lower-level (3) and upper-level (2) optimization problems in BiSSL. The lower-level training optimizes the pretext task objective, while additionally including the gradient of the regularization term r for the backbone parameter updates, complying with (3). For the upper-level training, the gradient with respect to the backbone parameters as represented by the left term on the right-hand side in (7), is approximated using the CG method. This algorithm is applicable to any common pretext and downstream tasks, with the only supplementary requirement being that the pretext task objective is twice-differentiable.

From Section A.1 in Appendix A, we get that $\boldsymbol{\theta}_P^*(\boldsymbol{\theta}_D)$ must fulfill the stationary condition $\nabla_{\boldsymbol{\theta}} (\mathcal{L}^P(\boldsymbol{\theta}, \phi_P) + \lambda r(\boldsymbol{\theta}_D, \boldsymbol{\theta}))|_{\boldsymbol{\theta}=\boldsymbol{\theta}_P^*(\boldsymbol{\theta}_D)} = \mathbf{0}$ to justify the explicit expression of the implicit gradient in (6). This means that executing Algorithm 1 using random initializations of $\boldsymbol{\theta}$ and ϕ_P will likely not suffice. The same applies to ϕ_D , as a random initialization of ϕ_D typically leads to rapid initial changes of the backbone parameters $\boldsymbol{\theta}_D$ during fine-tuning. This would then likely violate the assumed stationary condition due to the dependence between $\boldsymbol{\theta}_D$ and $\boldsymbol{\theta}_P$ through the regularization objective

r . Figure 1 illustrates the suggested pipeline alongside the conventional SSL pipeline. First, conventional pretext pre-training is performed on the unlabeled dataset \mathcal{D}^P to obtain initializations of θ and ϕ_P . Next, the downstream head is fitted on top of the frozen backbone θ using the downstream dataset \mathcal{D}^D , which provides an initialization of the downstream head parameters ϕ_D . Then, BiSSL training is conducted as outlined in Algorithm 1, yielding an updated configuration of backbone parameters $\theta_P^*(\theta_D)$. These updated backbone parameters are subsequently used as an initialization for the final supervised fine-tuning on the downstream task.

Algorithm 1 BiSSL Training Algorithm

Input: Backbone and pretext head initializations θ , ϕ_P , ϕ_D . Training objectives \mathcal{L}^P , \mathcal{L}^D . Optimizers opt_P , opt_D . Regularization Weight $\lambda \in \mathbb{R}_+$. Number of training stage alternations $T \in \mathbb{N}$ with upper and lower-level iterations $N_U, N_L \in \mathbb{N}$.

Initialize $\theta_P \leftarrow \theta$ and $\theta_D \leftarrow \theta$.

for $t = 1, \dots, T$ **do**

{Lower-level}

for $n = 1, \dots, N_L$ **do**

$$\mathbf{g}_{\phi_P} = \nabla_{\phi} \mathcal{L}^P(\theta_P, \phi_P).$$

$$\mathbf{g}_{\theta_P} = \nabla_{\theta} \mathcal{L}^P(\theta_P, \phi_P) + \lambda(\theta_P - \theta_D).$$

Update $\phi_P \leftarrow \text{opt}_P(\phi_P, \mathbf{g}_{\phi_P})$.

Update $\theta_P \leftarrow \text{opt}_P(\theta_P, \mathbf{g}_{\theta_P})$.

end for

{Upper-level}

for $n = 1, \dots, N_U$ **do**

$$\mathbf{g}_{\phi_D} = \nabla_{\phi} \mathcal{L}^D(\theta_P, \phi_D) + \nabla_{\phi} \mathcal{L}^D(\theta_D, \phi_D).$$

$$\mathbf{v} = \nabla_{\theta} \mathcal{L}^D(\theta_P, \phi_D).$$

{Use CG to approximate:}

$$\mathbf{v}_{\text{IG}} \approx [I_M + \frac{1}{\lambda} \nabla_{\theta}^2 \mathcal{L}^P(\theta_P, \phi_P)]^{-1} \mathbf{v}.$$

$$\mathbf{g}_{\theta_D} = \mathbf{v}_{\text{IG}} + \nabla_{\theta} \mathcal{L}^D(\theta_D, \phi_D).$$

Update $\phi_D \leftarrow \text{opt}_D(\phi_D, \mathbf{g}_{\phi_D})$.

Update $\theta_D \leftarrow \text{opt}_D(\theta_D, \mathbf{g}_{\theta_D})$.

end for

end for

Return: Backbone Parameters θ_P .

4. Experiments and Results

4.1. Datasets

The ImageNet-1K (Deng et al., 2009) dataset devoid of labels is used for self-supervised pre-training throughout the main experiments. For downstream fine-tuning and evaluation, we leverage a varied set of natural image classification datasets that encompass a wide array of

tasks, including general image classification, fine-grained recognition across species and objects, scene understanding, and texture categorization. The datasets include Food 101 (Bossard et al., 2014), CIFAR10 (Krizhevsky, 2012), CIFAR100 (Krizhevsky, 2012), Caltech-UCSD Birds-200-2011 (CUB200) (Wah et al., 2011), SUN397 scene dataset (Xiao et al., 2010), StanfordCars (Yang et al., 2015), FGVC Aircraft (Maji et al., 2013), PASCAL VOC 2007 (Everingham et al., 2010), Describable Textures Dataset (DTD) (Cimpoi et al., 2014), Oxford-IIIT Pets (Parkhi et al., 2012), Caltech-101 (Li et al., 2022a) and Oxford 102 Flowers (Nilsback & Zisserman, 2008). All downstream datasets are split into training, validation, and test partitions, with details on how these assignments are made provided in Section B.1 of Appendix B.

4.2. Implementation Details

4.2.1. BASELINE SETUP

Pretext Task Training We conduct experiments using two different types of pretext tasks: SimCLR Chen et al. (2020b) and Bootstrap Your Own Latent (BYOL) Grill et al. (2020). For SimCLR we use a temperature of 0.5 and a ResNet-50 He et al. (2016) backbone. On top of the backbone, a projection head is applied, consisting of two fully connected layers with batch normalization (Ioffe & Szegedy, 2015) and ReLU (Agarap, 2018) followed by a single linear layer. Each layer consists of 256 neurons. For BYOL, we use constant target decay rate of 0.9995, with the backbone and projection head architectures identical to those of SimCLR. The additional BYOL-specific prediction head uses an architecture identical to the projection head. The remaining details in this paragraph apply to both SimCLR and BYOL.

The image augmentation scheme follows the approach used in Bardes et al. (2022), with minor modifications: The image size is set to 96×96 instead of 224×224 , and the minimal ratio of the random crop is adjusted accordingly to 0.5 instead of 0.08.

The implementation of the LARS optimizer (You et al., 2017) from Bardes et al. (2022) is employed, with a ‘‘trust’’ coefficient of 0.001, a weight decay of 10^{-6} and a momentum of 0.9. The learning rate increases linearly during the first 10 epochs, reaching a peak base learning rate of 4.8, followed by a cosine decay with no restarts (Loshchilov & Hutter, 2017) for the remaining epochs. A batch size of 1024 is used and, unless otherwise specified, pre-training is conducted for 500 epochs.

Fine-Tuning on the Downstream Task For downstream fine-tuning, a single linear layer is attached to the output of the pre-trained backbone. The training procedure utilizes the cross-entropy loss, the SGD optimizer with a momentum of 0.9, and a cosine decaying learning rate scheduler

Table 1. Comparison of classification accuracies between the conventional SSL pipeline and our proposed BiSSL pipeline. Accuracies that are significantly higher from their counterparts are marked in bold font.

	Food	CIFAR10	CIFAR100	CUB200	SUN397	Cars	Aircrafts	VOC07	DTD	Pets	Caltech101	Flowers
SimCLR:												
Only FT	75.0 ± 0.1	96.1 ± 0.2	79.5 ± 0.2	49.6 ± 0.3	49.3 ± 0.2	78.0 ± 0.3	52.0 ± 1.0	*71.0 ± 0.1	60.3 ± 0.9	73.2 ± 0.3	85.7 ± 0.5	82.6 ± 0.3
BiSSL+FT	75.6 ± 0.1	96.4 ± 0.1	80.0 ± 0.1	59.2 ± 0.2	51.4 ± 0.2	78.0 ± 0.3	55.3 ± 0.5	*71.8 ± 0.1	63.4 ± 0.3	79.6 ± 0.3	88.1 ± 0.3	85.6 ± 0.2
Avg Diff	+0.6	+0.3	+0.5	+9.6	+2.1	0.0	+3.3	+0.8	+3.1	+6.4	+2.4	+3.0
BYOL:												
Only FT	75.3 ± 0.2	96.4 ± 0.1	80.1 ± 0.2	52.7 ± 0.4	47.9 ± 0.3	76.9 ± 0.2	51.6 ± 0.7	*69.3 ± 0.1	59.5 ± 0.4	77.9 ± 0.3	86.6 ± 0.4	82.2 ± 0.5
BiSSL+FT	75.4 ± 0.1	96.4 ± 0.1	80.6 ± 0.1	60.1 ± 0.1	50.2 ± 0.2	78.1 ± 0.3	57.1 ± 0.4	*71.1 ± 0.1	62.2 ± 0.1	81.9 ± 0.1	88.3 ± 0.3	86.5 ± 0.1
Avg Diff	+0.1	0.0	+0.5	+7.4	+2.3	+1.2	+5.5	+1.8	+2.7	+4.0	+1.7	+4.3

without restarts (Loshchilov & Hutter, 2017). Fine-tuning is conducted for 400 epochs with a batch size of 256. An augmentation scheme similar to the fine-tuning augmentation scheme in Bardes et al. (2022) is employed during training, where images are center cropped and resized to 96×96 pixels with a minimal crop ratio of 0.5, followed by random horizontal flips.

A random grid search of 100 hyper-parameter configurations for the base learning rates and weight decays is conducted, where one model is fine-tuned for each configuration. Base learning rates and weight decays are log-uniformly sampled over the ranges of 0.0001 to 1.0 and 0.00001 to 0.01, respectively. Validation data accuracy is evaluated after each epoch. The hyper-parameter configuration yielding the best balance between high validation accuracy and low validation loss is considered the optimal hyper-parameter configuration.² The corresponding optimal hyper-parameters for each downstream dataset are documented in Table 3 of Appendix B.

For subsequent evaluation on the test data, we train 10 models with different random seeds, each using the considered optimal hyper-parameter configurations. During the training of each respective model, the model parameters are stored after each epoch if the top-1 validation accuracy (or 11-point mAP for the VOC07 dataset) has increased compared to the previous highest top-1 validation accuracy achieved during training. Top-1 and top-5 test data accuracies (or 11-point mAP for the VOC07 dataset) are evaluated for each of the 10 models, from which the calculated means and standard deviations of these accuracies are documented.

4.2.2. BiSSL SETUP

In this section, we detail each stage of the proposed training pipeline for BiSSL, as outlined in the right part of Figure 1.

Pretext Task The backbone θ and projection head ϕ_P are initialized by self-supervised pre-training using a setup

²In certain scenarios during the experiments, the configuration that achieved the highest validation accuracy also yielded a notably higher relative validation loss. To ensure better generalizability, an alternative configuration with a more favorable trade-off was selected in these cases.

identical to the baseline pretext task training setup detailed in Section 4.2.1. This enables reusing the pre-trained backbones from the baseline experiments.

Downstream Head Warm-up The training setup for the downstream head warm-up closely mirrors the fine-tuning setup of Section 4.2.1. The main difference is that only the linear downstream head is fitted on top of the now frozen backbone obtained from the pretext warm-up. Learning rates and weight decays are initially selected based on those listed in Table 3, with adjustments made as needed when preliminary testing indicated a potential for improved convergence. These values are provided in Table 4 in Appendix B. The authors recognize that more optimal hyper-parameter configurations may exist and leave further exploration of this for future refinement. The downstream head warm-up is conducted for 20 epochs with a constant learning rate.

Lower-level of BiSSL The training configuration for the lower-level primarily follows the setup described for pretext pre-training in Section 4.2.1, with the modifications outlined here. As specified in (3), the lower-level loss function is the sum of the pretext task objective \mathcal{L}^P (e.g. the NT-Xent loss for SimCLR (Chen et al., 2020b)) and the regularization term $r(\theta_D, \theta_P) = \frac{1}{2} \|\theta_D - \theta_P\|_2^2$, aligning with Algorithm 1. Based on early experiments, the regularization weight $\lambda = 0.001$ was selected, as it appeared to strike a well-balanced compromise between the convergence rates of both the lower- and upper-level objectives. The lower-level is trained for the equivalent of approximately 8 conventional pre-training epochs, with further details provided in the composite configuration paragraph. Accordingly the linear learning rate scheduler warm-up is adjusted to range over $10 \cdot N_L$ training steps, with N_L being the number of lower-level iterations as specified in Algorithm 1.

Upper-level of BiSSL The upper-level training stage also shares many similarities with the downstream training setup described in Section 4.2.1, and again, only the differences are addressed here. The weight decays and base learning rates are set to match those obtained from the downstream head warm-up detailed in Table 4 of Appendix B. To approximate the upper-level gradient in (7), the conjugate

Table 2. Comparison of AP₅₀-scores for object detection on the VOC07+12 dataset using a Faster-RCNN with a R50-C4 backbone.

	SimCLR	BYOL
Only FT	59.6 ± 0.3	54.6 ± 0.5
BiSSL+FT	60.6 ± 0.1	56.7 ± 0.4

gradient method (Nazareth, 2009; Shewchuk, 1994) is employed, with implementation details covered in Section B.3 of Appendix B.

Composite Configuration Details of BiSSL As outlined in Algorithm 1, both lower- and upper-level backbone parameters θ_P and θ_D are initialized with the backbone parameters obtained during the pretext warm-up, and the training procedure alternates between solving the lower- and upper-level optimization problems. In this experimental setup, the lower-level performs $N_L = 20$ gradient steps before alternating to the upper-level, which then conducts $N_U = 8$ gradient steps. A total of $T = 500$ training stage alternations are executed. With the ImageNet dataset and the current batch size of 1024, there are a total of 1251 training batches without replacement. Consequently, the $T = 500$ training stage alternations correspond to roughly 8 conventional pretext epochs, a negligible additional training load compared to the 500 pretext epochs used for the full pre-training process. Additionally, gradient normalization is employed on gradients exceeding ℓ_2 -norms of 10.

Fine-Tuning on the Downstream Task Subsequent downstream fine-tuning is conducted in a manner identical to that described in the “Fine-Tuning on the Downstream Task” paragraph of section 4.2.1. Table 5 in Appendix B lists the considered optimal hyper-parameter configurations for each dataset.

4.3. Downstream Task Performance

We first assess the impact of using BiSSL compared to the conventional self-supervised training pipeline by evaluating classification accuracies on the various specified downstream datasets. Table 1 report means and standard deviations of top-1 classification accuracies (or the 11-point mAP on the VOC2007 dataset), comparing results obtained from the conventional SSL pipeline with those achieved using the BiSSL pipeline. Table 6 of Section C.1 in Appendix C outlines the corresponding top-5 accuracies. The results reveal BiSSL significantly improves downstream performance on 10 out of 12 datasets, with no single result showing a decline in performance compared to the baseline. Moreover, classification accuracies achieved via BiSSL exhibit greater stability, as evidenced by consistently lower or comparable variances relative to the baseline.

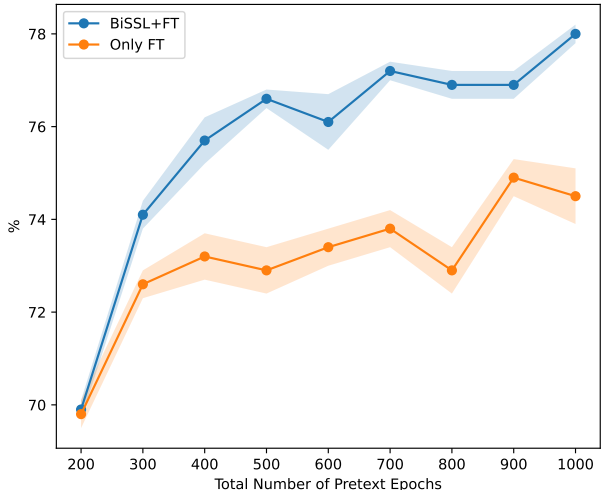


Figure 2. Top-1 test classification accuracies on the Flowers dataset for separate models pre-trained with SimCLR for different durations, comparing the conventional and BiSSL training pipelines. BiSSL consistently achieves significantly higher accuracies than the baseline after sufficient pre-training.

4.3.1. OBJECT DETECTION

To assess if the advantages of BiSSL extend beyond classification tasks, we further assess its performance in the context of object detection. Similarly to the setup of Bardes et al. (2022); He et al. (2020), we use a Faster-RCNN with a ResNet-50 C4 backbone (Ren et al., 2015) on the VOC07+12 (Everingham et al., 2010) dataset and report the standard AP₅₀ metric. We refer to Section B.6 in Appendix B for additional implementation details. The results presented in Table 2 support the previous conclusions, indicating that BiSSL enhances downstream performance.

4.3.2. VARYING THE PRE-TRAINING DURATION

To further assess the robustness of BiSSL, we conduct experiments varying the duration of self-supervised pre-training. Given the limitations of the computational resources available for this work, we adopt a smaller-scale version of the SimCLR setup, by instead using a ResNet-18 backbone and the unlabeled partition of the smaller-scale STL10 Coates et al. (2011) dataset for pre-training. The rest of the experimental setup remains largely unchanged, except for the following remark. The BiSSL training stage with the previously specified parameters from Section 4.2.2 is now approximately equal to conducting 100 conventional pretext epochs. Consequently, we compare BiSSL with baselines pre-trained for 100 additional epochs to ensure the total pretext training duration is approximately equal across methods, enabling a fair evaluation. The Flowers classification dataset,

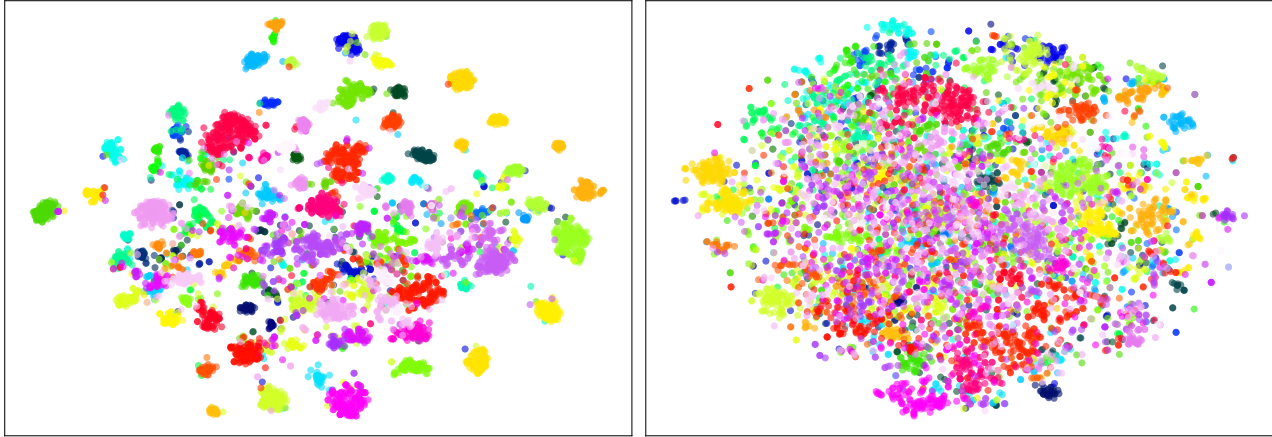


Figure 3. Visualization of features from a lower-level backbone obtained after applying BiSSL (left) and a backbone trained using pretext pre-training exclusively (right). Features are extracted from the test partition of the flowers dataset and each color represents a different class. Details are outlined in Section C.2 of Appendix C

which demonstrated substantial benefits from BiSSL was chosen for these experiments. Figure 2 depicts the final fine-tuned test accuracy achieved by separate models pre-trained for varying durations. The results show that BiSSL consistently outperforms the baseline once a sufficient duration of pre-training is reached, aligning with the remarks in Section 3.4. This suggests that the BiSSL’s benefits are not contingent on the amount of pre-training, but rather support the notion that it provides a more efficient learning trajectory, stemming from the enhanced information sharing it facilitates between the pretext and downstream tasks.

4.4. Visual Inspection of Latent Features

To gain deeper insight into how BiSSL affects the representations learned compared to conventional pretext pre-training, we perform a qualitative visual inspection of latent spaces. This involves comparing features processed by backbones trained solely by pretext pre-training using SimCLR to those derived from lower-level backbones obtained after conducting BiSSL, each trained as described in the “Pretext Task Training” and “Lower-level of BiSSL” paragraphs in Section 4.2.1 and 4.2.2, respectively. By comparing these features, we aim to assess whether BiSSL nudges the latent features toward being more semantically meaningful for the downstream task. The t-Distributed Stochastic Neighbor Embedding (t-SNE) (Cieslak et al., 2020) technique is employed for dimensionality reduction. Further details regarding the experimental setup are outlined in Section C.2 of Appendix C. Figure 3 illustrates the results on the flowers dataset, indicating that BiSSL yields backbones with improved downstream feature alignment. Further plots on a selection of downstream datasets in Section C.2 reinforce

this finding, also demonstrating that this trend consistently persists even for datasets where BiSSL did not impose any classification accuracy improvements.

5. Conclusion

This study integrates pretext pre-training and downstream fine-tuning into a unified bilevel optimization problem, from which the BiSSL training framework is proposed. BiSSL explicitly models the inheritance of backbone parameters from the pretext task, improving the transfer of relevant information between pretext and downstream tasks. We propose a task-agnostic training algorithm and pipeline that incorporates BiSSL as an intermediate stage between pretext pre-training and downstream fine-tuning. Experiments across multiple pretext and downstream tasks demonstrate that BiSSL delivers significant downstream performance improvements over the conventional self-supervised learning pipeline. Qualitative inspections of latent spaces further supports the notion that BiSSL enhances downstream task alignment. BiSSL marks a promising development toward better aligning the pretext pre-training and downstream fine-tuning stages, revealing a new direction for self-supervised learning algorithm designs that leverage bilevel optimization.

Acknowledgments

This project is supported by the Pioneer Centre for Artificial Intelligence, Denmark.³ The authors would like to thank Sijia Liu and Yihua Zhang (Michigan State University) pro-

³<https://www.aicentre.dk>

viding valuable feedback in a discussion, which helped to refine and solidify our perspective on the topic of integrating bilevel optimization in deep learning.

Impact Statement

This paper presents work whose goal is to advance the field of Machine Learning. There are many potential societal consequences of our work, none which we feel must be specifically highlighted here.

References

- Agarap, A. F. Deep learning using rectified linear units (relu). *arXiv preprint arXiv:1803.08375*, 2018.
- Arjovsky, M., Bottou, L., Gulrajani, I., and Lopez-Paz, D. Invariant risk minimization. *ArXiv*, abs/1907.02893, 2019.
- Baevski, A., Zhou, Y., Mohamed, A., and Auli, M. wav2vec 2.0: A framework for self-supervised learning of speech representations. *Advances in neural information processing systems*, 33:12449–12460, 2020.
- Bardes, A., Ponce, J., and LeCun, Y. VICReg: Variance-invariance-covariance regularization for self-supervised learning. In *International Conference on Learning Representations*, 2022.
- Boonlia, H., Dam, T., Ferdaus, M. M., Anavatti, S. G., and Mullick, A. Improving self-supervised learning for out-of-distribution task via auxiliary classifier. In *2022 IEEE International Conference on Image Processing (ICIP)*, pp. 3036–3040. IEEE, 2022.
- Borsos, Z., Mutny, M., and Krause, A. Coresets via bilevel optimization for continual learning and streaming. *Advances in neural information processing systems*, 33:14879–14890, 2020.
- Boschini, M., Bonicelli, L., Porrello, A., Bellitto, G., Pennisi, M., Palazzo, S., Spampinato, C., and Calderara, S. Transfer without forgetting. In *European Conference on Computer Vision*, pp. 692–709. Springer, 2022.
- Bossard, L., Guillaumin, M., and Van Gool, L. Food-101 – mining discriminative components with random forests. In *European Conference on Computer Vision*, 2014.
- Brown, T., Mann, B., Ryder, N., Subbiah, M., Kaplan, J. D., Dhariwal, P., Neelakantan, A., Shyam, P., Sastry, G., Askell, A., Agarwal, S., Herbert-Voss, A., Krueger, G., Henighan, T., Child, R., Ramesh, A., Ziegler, D., Wu, J., Winter, C., Hesse, C., Chen, M., Sigler, E., Litwin, M., Gray, S., Chess, B., Clark, J., Berner, C., McCandlish, S., Radford, A., Sutskever, I., and Amodei, D. Language models are few-shot learners. In Larochelle, H., Ranzato, M., Hadsell, R., Balcan, M., and Lin, H. (eds.), *Advances in Neural Information Processing Systems*, volume 33, pp. 1877–1901. Curran Associates, Inc., 2020.
- Caron, M., Misra, I., Mairal, J., Goyal, P., Bojanowski, P., and Joulin, A. Unsupervised learning of visual features by contrasting cluster assignments. *Advances in neural information processing systems*, 33:9912–9924, 2020.
- Caron, M., Touvron, H., Misra, I., Jegou, H., Mairal, J., Bojanowski, P., and Joulin, A. Emerging properties in self-supervised vision transformers. In *2021 IEEE/CVF International Conference on Computer Vision (ICCV)*, pp. 9630–9640, 2021. doi: 10.1109/ICCV48922.2021.00951.
- Chang, H.-J., Liu, A. H., and Glass, J. Self-supervised Fine-tuning for Improved Content Representations by Speaker-invariant Clustering. In *INTERSPEECH 2023*, pp. 2983–2987. ISCA, August 2023. doi: 10.21437/Interspeech.2023-847.
- Chen, S., Hou, Y., Cui, Y., Che, W., Liu, T., and Yu, X. Recall and learn: Fine-tuning deep pretrained language models with less forgetting. In Webber, B., Cohn, T., He, Y., and Liu, Y. (eds.), *EMNLP (1)*, pp. 7870–7881. Association for Computational Linguistics, 2020a. ISBN 978-1-952148-60-6.
- Chen, T., Kornblith, S., Norouzi, M., and Hinton, G. A simple framework for contrastive learning of visual representations. In *International conference on machine learning*, pp. 1597–1607. PMLR, 2020b.
- Choe, S. K., Neiswanger, W., Xie, P., and Xing, E. Betty: An automatic differentiation library for multilevel optimization. In *The Eleventh International Conference on Learning Representations*, 2023. URL https://openreview.net/forum?id=LV_MeMS38Q9.
- Chung, Y.-A. and Glass, J. Speech2Vec: A Sequence-to-Sequence Framework for Learning Word Embeddings from Speech. In *Proc. Interspeech 2018*, pp. 811–815, 2018. doi: 10.21437/Interspeech.2018-2341.
- Chung, Y.-A., Hsu, W.-N., Tang, H., and Glass, J. An Unsupervised Autoregressive Model for Speech Representation Learning. In *Proc. Interspeech 2019*, pp. 146–150, 2019. doi: 10.21437/Interspeech.2019-1473.
- Cieslak, M. C., Castelfranco, A. M., Roncalli, V., Lenz, P. H., and Hartline, D. K. t-distributed stochastic neighbor embedding (t-sne): A tool for eco-physiological transcriptomic analysis. *Marine Genomics*, 51:100723, 2020. ISSN 1874-7787. doi: <https://doi.org/10.1016/j.margen.2019.100723>.

- Cimpoi, M., Maji, S., Kokkinos, I., Mohamed, S., , and Vedaldi, A. Describing textures in the wild. In *Proceedings of the IEEE Conf. on Computer Vision and Pattern Recognition (CVPR)*, 2014.
- Coates, A., Ng, A., and Lee, H. An analysis of single-layer networks in unsupervised feature learning. In Gordon, G., Dunson, D., and Dudík, M. (eds.), *Proceedings of the Fourteenth International Conference on Artificial Intelligence and Statistics*, volume 15 of *Proceedings of Machine Learning Research*, pp. 215–223, Fort Lauderdale, FL, USA, 11–13 Apr 2011. PMLR.
- Deng, J., Dong, W., Socher, R., Li, L.-J., Li, K., and Fei-Fei, L. Imagenet: A large-scale hierarchical image database. In *2009 IEEE Conference on Computer Vision and Pattern Recognition*, pp. 248–255, 2009. doi: 10.1109/CVPR.2009.5206848.
- Devlin, J., Chang, M.-W., Lee, K., and Toutanova, K. Bert: Pre-training of deep bidirectional transformers for language understanding. In *North American Chapter of the Association for Computational Linguistics*, 2019.
- Donahue, J., Jia, Y., Vinyals, O., Hoffman, J., Zhang, N., Tzeng, E., and Darrell, T. Decaf: A deep convolutional activation feature for generic visual recognition. In Xing, E. P. and Jebara, T. (eds.), *Proceedings of the 31st International Conference on Machine Learning*, volume 32 of *Proceedings of Machine Learning Research*, pp. 647–655, Beijing, China, 22–24 Jun 2014. PMLR.
- Dontchev, A. and Rockafellar, R. *Implicit Functions and Solution Mappings: A View from Variational Analysis*. Springer Series in Operations Research and Financial Engineering. Springer New York, 2014. ISBN 9781493910373.
- Dubois, Y., Hashimoto, T., Ermon, S., and Liang, P. Improving self-supervised learning by characterizing idealized representations. *ArXiv*, abs/2209.06235, 2022.
- Everingham, M., Gool, L. V., Williams, C. K. I., Winn, J. M., and Zisserman, A. The pascal visual object classes (voc) challenge. *Int. J. Comput. Vis.*, 88(2):303–338, 2010.
- Fan, C., Ram, P., and Liu, S. Sign-MAML: Efficient model-agnostic meta-learning by signSGD. In *Fifth Workshop on Meta-Learning at the Conference on Neural Information Processing Systems*, 2021.
- Finn, C., Abbeel, P., and Levine, S. Model-agnostic meta-learning for fast adaptation of deep networks. In *International Conference on Machine Learning*, 2017.
- Franceschi, L., Frasconi, P., Salzo, S., Grazzi, R., and Pontil, M. Bilevel programming for hyperparameter optimization and meta-learning. In *International conference on machine learning*, pp. 1568–1577. PMLR, 2018.
- Grill, J.-B., Strub, F., Alché, F., Tallec, C., Richemond, P., Buchatskaya, E., Doersch, C., Avila Pires, B., Guo, Z., Gheshlaghi Azar, M., et al. Bootstrap your own latent-a new approach to self-supervised learning. *Advances in neural information processing systems*, 33:21271–21284, 2020.
- Gupta, K., Ajanthan, T., van den Hengel, A., and Gould, S. Understanding and improving the role of projection head in self-supervised learning. *ArXiv*, abs/2212.11491, 2022.
- He, K., Zhang, X., Ren, S., and Sun, J. Deep residual learning for image recognition. In *Proceedings of the IEEE conference on computer vision and pattern recognition*, pp. 770–778, 2016.
- He, K., Fan, H., Wu, Y., Xie, S., and Girshick, R. Momentum contrast for unsupervised visual representation learning. In *Proceedings of the IEEE/CVF conference on computer vision and pattern recognition*, pp. 9729–9738, 2020.
- He, K., Chen, X., Xie, S., Li, Y., Dollár, P., and Girshick, R. Masked autoencoders are scalable vision learners. In *Proceedings of the IEEE/CVF conference on computer vision and pattern recognition*, pp. 16000–16009, 2022.
- He, P., Liu, X., Gao, J., and Chen, W. DeBERTa: Decoding-enhanced bert with disentangled attention. In *International Conference on Learning Representations*, 2021.
- Hsu, W.-N., Bolte, B., Tsai, Y.-H. H., Lakhota, K., Salakhutdinov, R., and Mohamed, A. Hubert: Self-supervised speech representation learning by masked prediction of hidden units. *IEEE/ACM Transactions on Audio, Speech, and Language Processing*, 29:3451–3460, 2021.
- Ioffe, S. and Szegedy, C. Batch normalization: Accelerating deep network training by reducing internal covariate shift. In *International conference on machine learning*, pp. 448–456. pmlr, 2015.
- Kirillov, A., Mintun, E., Ravi, N., Mao, H., Rolland, C., Gustafson, L., Xiao, T., Whitehead, S., Berg, A. C., Lo, W.-Y., Dollár, P., and Girshick, R. B. Segment anything. *2023 IEEE/CVF International Conference on Computer Vision (ICCV)*, pp. 3992–4003, 2023.
- Krizhevsky, A. Learning multiple layers of features from tiny images. *University of Toronto*, 05 2012.
- Lewis, M., Liu, Y., Goyal, N., Ghazvininejad, M., rahman Mohamed, A., Levy, O., Stoyanov, V., and Zettlemoyer, L. Bart: Denoising sequence-to-sequence pre-training for natural language generation, translation, and comprehension. In *Annual Meeting of the Association for Computational Linguistics*, 2019.

- Li, F.-F., Andreeto, M., Ranzato, M., and Perona, P. Caltech 101, Apr 2022a.
- Li, J., Qiang, W., Zhang, Y., Mo, W., Zheng, C., Su, B., and Xiong, H. Metamask: Revisiting dimensional confounder for self-supervised learning. *Advances in Neural Information Processing Systems*, 35:38501–38515, 2022b.
- Li, X., Xiong, H., An, H., Xu, C.-Z., and Dou, D. Rifle: Backpropagation in depth for deep transfer learning through re-initializing the fully-connected layer. In *International Conference on Machine Learning*, pp. 6010–6019. PMLR, 2020.
- Lorraine, J., Vicol, P., and Duvenaud, D. Optimizing millions of hyperparameters by implicit differentiation. In *International conference on artificial intelligence and statistics*, pp. 1540–1552. PMLR, 2020.
- Loshchilov, I. and Hutter, F. SGDR: Stochastic gradient descent with warm restarts. In *International Conference on Learning Representations*, 2017.
- Maji, S., Kannala, J., Rahtu, E., Blaschko, M., and Vedaldi, A. Fine-grained visual classification of aircraft. Technical report, 2013.
- Nazareth, J. L. Conjugate gradient method. *WIREs Computational Statistics*, 1(3):348–353, 2009. doi: <https://doi.org/10.1002/wics.13>.
- Niizumi, D., Takeuchi, D., Ohishi, Y., Harada, N., and Kashino, K. Byol for audio: Self-supervised learning for general-purpose audio representation. In *2021 International Joint Conference on Neural Networks (IJCNN)*, pp. 1–8. IEEE, 2021.
- Nilsback, M.-E. and Zisserman, A. Automated flower classification over a large number of classes. In *Indian Conference on Computer Vision, Graphics and Image Processing*, Dec 2008.
- Oquab, M., Darcet, T., Moutakanni, T., Vo, H. V., Szafraniec, M., Khalidov, V., Fernandez, P., HAZIZA, D., Massa, F., El-Nouby, A., Assran, M., Ballas, N., Galuba, W., Howes, R., Huang, P.-Y., Li, S.-W., Misra, I., Rabbat, M., Sharma, V., Synnaeve, G., Xu, H., Jegou, H., Mairal, J., Labatut, P., Joulin, A., and Bojanowski, P. DINOv2: Learning robust visual features without supervision. *Transactions on Machine Learning Research*, 2024. ISSN 2835-8856.
- Pan, H., Guo, Y., Deng, Q., Yang, H.-F., Chen, Y., and Chen, J. Improving fine-tuning of self-supervised models with contrastive initialization. *Neural networks : the official journal of the International Neural Network Society*, 159: 198–207, 2022.
- Parkhi, O. M., Vedaldi, A., Zisserman, A., and Jawahar, C. V. Cats and dogs. In *IEEE Conference on Computer Vision and Pattern Recognition*, 2012.
- Pedregosa, F. Hyperparameter optimization with approximate gradient. In Balcan, M. F. and Weinberger, K. Q. (eds.), *Proceedings of The 33rd International Conference on Machine Learning*, volume 48 of *Proceedings of Machine Learning Research*, pp. 737–746, New York, New York, USA, 20–22 Jun 2016. PMLR.
- Rajeswaran, A., Finn, C., Kakade, S. M., and Levine, S. Meta-learning with implicit gradients. In *Neural Information Processing Systems*, 2019.
- Ren, S., He, K., Girshick, R., and Sun, J. Faster r-cnn: Towards real-time object detection with region proposal networks. In Cortes, C., Lawrence, N., Lee, D., Sugiyama, M., and Garnett, R. (eds.), *Advances in Neural Information Processing Systems*, volume 28. Curran Associates, Inc., 2015.
- Schneider, S., Baeviski, A., Collobert, R., and Auli, M. wav2vec: Unsupervised Pre-Training for Speech Recognition. In *Proc. Interspeech 2019*, pp. 3465–3469, 2019. doi: 10.21437/Interspeech.2019-1873.
- Shewchuk, J. R. An introduction to the conjugate gradient method without the agonizing pain. Technical report, Carnegie Mellon University, 1994.
- Simonyan, K. and Zisserman, A. Very deep convolutional networks for large-scale image recognition. *arXiv preprint arXiv:1409.1556*, 2014.
- Touvron, H., Lavril, T., Izacard, G., Martinet, X., Lachaux, M.-A., Lacroix, T., Rozière, B., Goyal, N., Hambro, E., Azhar, F., et al. Llama: Open and efficient foundation language models. *arXiv preprint arXiv:2302.13971*, 2023.
- Wah, C., Branson, S., Welinder, P., Perona, P., and Belongie, S. The caltech-ucsd birds-200-2011 dataset. Technical Report CNS-TR-2011-001, California Institute of Technology, 2011.
- Wu, C., Wu, F., Qi, T., Huang, Y., and Xie, X. Noisy tune: A little noise can help you finetune pretrained language models better. In *Annual Meeting of the Association for Computational Linguistics*, 2022.
- Xiao, J., Hays, J., Ehinger, K. A., Oliva, A., and Torralba, A. Sun database: Large-scale scene recognition from abbey to zoo. In *2010 IEEE Computer Society Conference on Computer Vision and Pattern Recognition*, pp. 3485–3492, 2010. doi: 10.1109/CVPR.2010.5539970.
- Yadav, S., Theodoridis, S., Hansen, L. K., and Tan, Z.-H. Masked autoencoders with multi-window local-global

- attention are better audio learners. In *The Twelfth International Conference on Learning Representations*, 2024.
- Yang, L., Luo, P., Loy, C. C., and Tang, X. A large-scale car dataset for fine-grained categorization and verification. In *2015 IEEE Conference on Computer Vision and Pattern Recognition (CVPR)*, pp. 3973–3981, 2015. doi: 10.1109/CVPR.2015.7299023.
- You, Y., Gitman, I., and Ginsburg, B. Large batch training of convolutional networks. *arXiv: Computer Vision and Pattern Recognition*, 2017.
- Zaiem, S., Parcollet, T., and Essid, S. Less forgetting for better generalization: Exploring continual-learning finetuning methods for speech self-supervised representations. *arXiv preprint arXiv:2407.00756*, 2024.
- Zhai, X., Oliver, A., Kolesnikov, A., and Beyer, L. S4l: Self-supervised semi-supervised learning. *2019 IEEE/CVF International Conference on Computer Vision (ICCV)*, pp. 1476–1485, 2019.
- Zhang, L., Liang, Y., Zhang, R., Javadi, A., and Xie, P. BLO-SAM: Bi-level optimization based finetuning of the segment anything model for overfitting-preventing semantic segmentation. In Salakhutdinov, R., Kolter, Z., Heller, K., Weller, A., Oliver, N., Scarlett, J., and Berkenkamp, F. (eds.), *Proceedings of the 41st International Conference on Machine Learning*, volume 235 of *Proceedings of Machine Learning Research*, pp. 59289–59309. PMLR, 21–27 Jul 2024.
- Zhang, T., Qiu, C., Ke, W., Süssstrunk, S., and Salzmann, M. Leverage your local and global representations: A new self-supervised learning strategy. In *Proceedings of the IEEE/CVF Conference on Computer Vision and Pattern Recognition*, pp. 16580–16589, 2022a.
- Zhang, Y., Zhang, G., Khanduri, P., Hong, M.-F., Chang, S., and Liu, S. Revisiting and advancing fast adversarial training through the lens of bi-level optimization. In *International Conference on Machine Learning*, 2021.
- Zhang, Y., Yao, Y., Ram, P., Zhao, P., Chen, T., Hong, M., Wang, Y., and Liu, S. Advancing model pruning via bi-level optimization. In Koyejo, S., Mohamed, S., Agarwal, A., Belgrave, D., Cho, K., and Oh, A. (eds.), *Advances in Neural Information Processing Systems*, volume 35, pp. 18309–18326. Curran Associates, Inc., 2022b.
- Zhang, Y., Khanduri, P., Tsaknakis, I. C., Yao, Y., Hong, M.-F., and Liu, S. An introduction to bi-level optimization: Foundations and applications in signal processing and machine learning. *ArXiv*, abs/2308.00788, 2023a.
- Zhang, Y., Sharma, P., Ram, P., Hong, M., Varshney, K. R., and Liu, S. What is missing in IRM training and evaluation? challenges and solutions. In *The Eleventh International Conference on Learning Representations*, 2023b.
- Zucchet, N. and Sacramento, J. Beyond backpropagation: bilevel optimization through implicit differentiation and equilibrium propagation. *Neural Computation*, 34(12): 2309–2346, 2022.

A. Theoretical Insights and Framework Comparisons in BiSSL

A.1. Derivation of the Implicit Gradient

Assume the setup of the BiSSL optimization problem described in (2) and (3). In the following derivations, we will assume that ϕ_P is fixed, allowing us to simplify the expressions involved. To streamline the notation further, we continue to use the convention $\nabla_{\xi} h(\xi)|_{\xi=\psi} := \nabla_{\xi} h(\psi)$, when it is clear from context which variables are differentiated with respect to. Under these circumstances, we then define the lower-level objective from (3) as

$$G(\theta_D, \theta_P) := \mathcal{L}^P(\theta_P, \phi_P) + \lambda r(\theta_D, \theta_P). \quad (8)$$

Recalling that r is a *convex* regularization objective, adequate scaling of λ effectively ‘‘convexifies’’ the lower-level objective G , a strategy also employed on the lower-level objective in previous works (Rajeswaran et al., 2019; Zhang et al., 2022b; 2023a). This is advantageous because assuming convexity of G ensures that for any $\theta_D \in \mathbb{R}^L$, there exists a corresponding $\hat{\theta}_P \in \mathbb{R}^L$ that satisfies the stationary condition $\nabla_{\theta_P} G(\theta_D, \hat{\theta}_P) = \mathbf{0}$. In other words, we are assured that a potential minimizer of $G(\theta_D, \cdot)$ exists for all $\theta_D \in \mathbb{R}^L$. Now, further assume that the gradient $\nabla_{\theta_P} G(\theta_D, \theta_P)$ is continuously differentiable and that the Hessian matrix $\nabla_{\theta_P}^2 G(\theta_D, \hat{\theta}_P)$ is invertible for all $\theta_D \in \mathbb{R}^L$. Under these conditions, the implicit function theorem (Dontchev & Rockafellar, 2014; Zucchet & Sacramento, 2022) guarantees the existence of an implicit unique and *differentiable* function $\theta_P^* : \mathcal{N}(\theta_D) \rightarrow \mathbb{R}^L$, with $\mathcal{N}(\theta_D)$ being a neighborhood of θ_D , that satisfies $\theta_P^*(\theta_D) = \hat{\theta}_P$ and $\nabla_{\theta_P} G(\theta_D, \theta_P^*(\theta_D)) = \mathbf{0}$ for all $\theta_D \in \mathcal{N}(\theta_D)$.

As we then conclude that the lower-level solution $\theta_P^*(\theta_D)$ is indeed a differentiable function under these conditions, this justifies that the expression

$$\frac{d}{d\theta_D} \nabla_{\theta_P} [G(\theta_D, \theta_P^*(\theta_D))] = \mathbf{0}$$

is valid for all $\theta_D \in \mathbb{R}^L$. By applying the chain rule, the expression becomes

$$\nabla_{\theta_D \theta_P}^2 G(\theta_D, \theta_P^*(\theta_D)) + \frac{d\theta_P^*(\theta_D)}{d\theta_D} \nabla_{\theta_P}^2 G(\theta_D, \theta_P^*(\theta_D)) = \mathbf{0}.$$

Recalling that $\nabla_{\theta_P}^2 G(\theta_D, \theta_P^*(\theta_D))$ is assumed to be invertible, the IG $\frac{d\theta_P^*(\theta_D)}{d\theta_D}$ can be isolated

$$\frac{d\theta_P^*(\theta_D)}{d\theta_D} = -\nabla_{\theta_D \theta_P}^2 G(\theta_D, \theta_P^*(\theta_D)) [\nabla_{\theta_P}^2 G(\theta_D, \theta_P^*(\theta_D))]^{-1},$$

and by substituting the expression for G from (8), the expression becomes

$$\frac{d\theta_P^*(\theta_D)}{d\theta_D} = -\nabla_{\theta_D \theta_P}^2 r(\theta_D, \theta_P^*(\theta_D)) \left[\nabla_{\theta_P}^2 \left(\frac{1}{\lambda} \mathcal{L}^P(\theta_P^*(\theta_D), \phi_P) + r(\theta_D, \theta_P^*(\theta_D)) \right) \right]^{-1}. \quad (9)$$

To summarize, given the following assumptions:

- The lower-level pretext head parameters ϕ_P are fixed.
- G is convex such that $\nabla_{\theta_P} G(\theta_D, \theta_P^*(\theta_D)) = \mathbf{0}$ is fulfilled for every $\theta_D \in \mathbb{R}^L$.
- The Hessian matrix $\nabla_{\theta_P}^2 G(\theta_D, \theta_P^*(\theta_D))$ exists and is invertible for all $\theta_D \in \mathbb{R}^L$.

Then, the IG $\frac{d\theta_P^*(\theta_D)}{d\theta_D}$ can be explicitly expressed by (9). The authors acknowledge that an explicit expression for the IG without fixing ϕ_P is achievable, though this is left for future exploration.

A.2. Distinction from Bilevel Optimization in Meta-Learning

While bilevel optimization (BLO) has been applied in meta-learning frameworks such as MAML (Finn et al., 2017), Sign-MAML (Fan et al., 2021) and iMAML (Rajeswaran et al., 2019), BiSSL represents a distinct application and implementation

of BLO, tailored for the challenges of self-supervised learning (SSL). In the aforementioned works, BLO is primarily utilized to address few-shot learning scenarios, focusing on efficiently adapting models to new tasks with minimal labeled data. Conversely, BiSSL applies BLO to concurrently manage the more complex task of self-supervised pretext pre-training on unlabeled with downstream fine-tuning on labeled data. Another key distinction is that in meta-learning, the upper- and lower-level objectives are closely related, with the upper-level objective formulated as a summation of the lower-level tasks. In contrast, BiSSL involves fundamentally distinct objectives at each level, utilizing separate datasets and tasks for pre-training and fine-tuning. This design allows BiSSL to better align the pre-trained model with the requirements of a specific downstream task. Conversely, the BLO in meta-learning aims to broadly generalize across a wide range of tasks, prioritizing adaptability rather than task-specific optimization. Additionally, unlike BiSSL, the meta-learning frameworks discussed reinitialize the lower-level backbone parameters with a copy of the upper-level parameters at every iteration.

B. Experimental Details

B.1. Dataset Partitions

The Caltech-101 (Li et al., 2022a) dataset does not come with a pre-defined train/test split, so the same convention as previous works is followed (Chen et al., 2020b; Donahue et al., 2014; Simonyan & Zisserman, 2014), where 30 random images per class are selected for the training partition, and the remaining images are assigned for the test partition. For the DTD (Cimpoi et al., 2014) and SUN397 (Xiao et al., 2010) datasets, which offer multiple proposed train/test partitions, the first splits are used, consistent with the approach in Chen et al. (2020b).

For downstream hyperparameter optimization, portions of the training partitions from each respective labeled dataset are designated as validation datasets. The FGVC Aircraft (Maji et al., 2013), Oxford 102 Flowers (Nilsback & Zisserman, 2008), DTD, and Pascal VOC 2007 (Everingham et al., 2010) datasets already have designated validation partitions. For all the remaining labeled datasets, the validation data partitions are randomly sampled while ensuring that class proportions are maintained. Roughly 20% of the training data is allocated for validation.

B.2. Downstream Task Fine-Tuning of the Baseline Setup

In Table 3, the learning rates and weight decays used for each respective downstream dataset of the experiments described in Section 4.2.1 are outlined.

Table 3. Optimal hyper-parameter configurations used for downstream fine-tuning after conventional pretext pre-training.

Dataset	SimCLR		BYOL	
	Learning Rate	Weight Decay	Learning Rate	Weight Decay
Food	0.0167	0.00613	0.0513	0.00147
CIFAR10	0.0033	0.00158	0.0014	0.00106
CIFAR100	0.0027	0.00012	0.0023	0.00012
CUB200	0.0409	0.0084	0.0095	0.00594
SUN397	0.0069	0.00003	0.004	0.00003
Cars	0.0377	0.00454	0.115	0.00257
Aircrafts	0.0269	0.0038	0.0119	0.00333
VOC07	0.0054	0.0089	0.0032	0.00616
DTD	0.0514	0.0011	0.0114	0.00011
Pets	0.0378	0.00114	0.0044	0.00779
Caltech101	0.0131	0.00005	0.0069	0.00027
Flowers	0.2178	0.00046	0.035	0.00262

B.3. Downstream Head Warmup and Upper-level of BiSSL

Table 4 outlines the learning rates and weight decays used for the downstream head warm-up and upper-level of BiSSL of each respective downstream dataset, as described in the BiSSL experimental setup of Section 4.2.2. The first term of the

Table 4. Hyper-parameters used for the Downstream Head Warm-up and Upper-level of BiSSL.

Dataset	SimCLR		BYOL	
	Learning Rate	Weight Decay	Learning Rate	Weight Decay
Food	0.03	0.001	0.035	0.002
CIFAR10	0.015	0.001	0.01	0.001
CIFAR100	0.01	0.0001	0.01	0.001
CUB200	0.03	0.001	0.015	0.0001
SUN397	0.015	0.00005	0.01	0.00005
Cars	0.035	0.001	0.04	0.002
Aircrafts	0.03	0.005	0.015	0.003
VOC07	0.015	0.005	0.005	0.006
DTD	0.03	0.001	0.015	0.0001
Pets	0.03	0.001	0.02	0.002
Caltech101	0.03	0.0001	0.015	0.0002
Flowers	0.05	0.0005	0.035	0.002

upper-level gradient (7) is approximated using the Conjugate Gradient (CG) method (Nazareth, 2009; Shewchuk, 1994). Our implementation follows a similar structure to that used in Rajeswaran et al. (2019), employing $N_c = 5$ iterations and a dampening term $\lambda_{\text{damp}} = 10$. Given matrix A and vector \mathbf{v} , the CG method iteratively approximates $A^{-1}\mathbf{v}$, which requires evaluation of multiple matrix-vector products $A\mathbf{d}_1, \dots, A\mathbf{d}_{N_c}$. In practice, storing the matrix A (in our case, the Hessian $\nabla_{\theta_P}^2 \mathcal{L}^P(\theta_P^*(\theta_D), \phi_P)$) in its full form is often infeasible. Instead, a function that efficiently computes the required matrix-vector products instead of explicitly storing the matrix is typically utilized. For transparency, the function employed in our setup is detailed in Algorithm 2. This approach ensures that the output of the CG algorithm is an approximation of the inverse Hessian-vector product in the first term of Equation (7) as intended.

Algorithm 2 Hessian Vector Product Calculation f_H (To use in the CG Algorithm)

Input: Input vector \mathbf{v} . Model parameters θ_P, ϕ_P . Training objective \mathcal{L}^P . Lower-level data batch \mathbf{x} . Regularization weight λ and dampening λ_{damp} .

$$\begin{aligned}
 \pi(\theta_P) &\leftarrow (\nabla_{\theta} \mathcal{L}^P(\theta, \phi_P; \mathbf{x})|_{\theta=\theta_P})^T \mathbf{v} \\
 \mathbf{g} &\leftarrow \nabla_{\theta} \pi(\theta)|_{\theta=\theta_P} \quad \{\text{Memory efficient calculation of } \nabla_{\theta}^2 \mathcal{L}^P(\theta, \phi_P; \mathbf{x})|_{\theta=\theta_P} \mathbf{x}\} \\
 \mathbf{y} &\leftarrow \mathbf{v} + \frac{1}{\lambda + \lambda_{\text{damp}}} \mathbf{g}
 \end{aligned}$$

Return: $f_H(\mathbf{v}) := \mathbf{y}$

B.4. Composite Configuration of BiSSL

To avoid data being reshuffled between every training stage alternation, the respective batched lower- and upper-level training datasets are stored in separate stacks from which data is drawn. The stacks are only “reset” when the number of remaining batches is smaller than the number of gradient steps required before alternating to the other level. For example, the lower-level stack is reshuffled every fourth training stage alternation. If the downstream dataset does not provide enough data for making $N_U = 8$ batches with non-overlapping data points, the data is simply reshuffled every time the remaining number of data points is smaller than the upper-level batch size (e.g. 256 images in the classification experiments).

Table 5. Optimal hyper-parameter configurations used for downstream fine-tuning after BiSSL.

Dataset	SimCLR		BYOL	
	Learning Rate	Weight Decay	Learning Rate	Weight Decay
Food	0.0037	0.00018	0.0496	0.00096
CIFAR10	0.001	0.00278	0.0018	0.00014
CIFAR100	0.0019	0.00002	0.0008	0.0013
CUB200	0.0005	0.00331	0.0007	0.00947
SUN397	0.0015	0.00001	0.0009	0.00062
Cars	0.0289	0.0075	0.0316	0.00632
Aircrafts	0.0002	0.0059	0.0003	0.00001
VOC07	0.0002	0.00019	0.0004	0.0003
DTD	0.0003	0.00002	0.0013	0.0021
Pets	0.0014	0.00005	0.0002	0.00039
Caltech101	0.0016	0.00042	0.0005	0.00022
Flowers	0.0189	0.00143	0.0057	0.00207

B.5. Downstream Fine-Tuning after BiSSL

The learning rates and weight decays used for downstream fine-tuning after BiSSL for each respective downstream dataset are outlined in Table 5. Section 4.2.2 outlines the experimental setup.

B.6. Object Detection

The experimental setup primarily follows the main implementation specified in Section 4.2, with minor modifications specified here.

We utilize a Faster R-CNN with a ResNet-50 C4 backbone (Ren et al., 2015) as the downstream model. The downstream data augmentations involve rescaling the images so that their longest edge is between 196 and 320 pixels, followed by normalization. Downstream fine-tuning is conducted for 50 epochs with a batch size of 16. The random hyperparameter grid search is performed across 50 distinct configurations of learning rates and weight decays, sampled log-uniformly within the intervals 10^{-4} to 10^{-1} and 10^{-6} to 10^{-2} , respectively.

Important for the context of BiSSL, we extend the pretext head parameters ϕ_P to further include the latter parameters of the ResNet-50 that are not part of the ResNet-50 C4 backbone. Lastly, the linear head warm-up is conducted for 5 epochs.

C. Additional Results

C.1. Top-5 Classification Accuracies

Table 6 outlines the corresponding top-5 accuracies of the experiments described in Section 4.3, which re-emphasizes the performance improvements imposed by BiSSL as initially implied by Table 1. Likewise Figure 4, outlines the corresponding top-5 accuracies of the experiments described in Section 4.3.2.

C.2. Visual inspection of Latent Features

Test data features of the downstream test data processed by backbones trained through conventional pretext pre-training with SimCLR are compared against those additionally trained with BiSSL. This allows for an inspection of the learned representations prior to the final fine-tuning stage.

During the evaluation, it is important to note that the batch normalization layers (Ioffe & Szegedy, 2015) of the pre-trained backbones utilize the running mean and variance inferred during training. Since these pre-trained backbones have not been exposed to the downstream datasets during training, their batch normalization statistics may not be optimal for these new datasets. To address this, the downstream training dataset is divided into batches of 256 samples, and roughly 100 batches

Table 6. Comparison of top-5 classification accuracies between the conventional SSL pipeline and our proposed BiSSL pipeline. Accuracies that are significantly higher from their counterparts are marked in bold font. Table 1 outlines the top-1 accuracies (and 11-point mAP for the VOC07 dataset).

	Food	CIFAR10	CIFAR100	CUB200	SUN397	Cars	Aircrafts	DTD	Pets	Caltech101	Flowers
SimCLR:											
Only FT	91.3 ± 0.1	100.0 ± 0.0	96.4 ± 0.1	75.2 ± 0.4	79.4 ± 0.4	93.7 ± 0.2	81.8 ± 0.5	85.8 ± 0.6	94.8 ± 0.4	98.1 ± 0.1	94.5 ± 0.2
BiSSL+FT	93.1 ± 0.1	100.0 ± 0.0	96.9 ± 0.1	86.5 ± 0.2	81.5 ± 0.1	93.7 ± 0.1	85.0 ± 0.2	88.7 ± 0.3	96.5 ± 0.1	98.7 ± 0.1	95.8 ± 0.1
Avg Diff	+1.8	0.0	+0.5	+11.3	+2.1	0.0	+3.2	+2.9	+1.7	+0.6	+1.3
BYOL:											
Only FT	91.8 ± 0.1	100.0 ± 0.0	96.3 ± 0.1	77.5 ± 0.4	77.8 ± 0.3	93.9 ± 0.2	81.8 ± 0.6	84.9 ± 0.4	95.6 ± 0.2	98.0 ± 0.1	93.6 ± 0.3
BiSSL+FT	91.8 ± 0.2	100.0 ± 0.0	96.7 ± 0.1	86.7 ± 0.2	80.1 ± 0.2	94.1 ± 0.2	87.5 ± 0.3	87.7 ± 0.3	97.2 ± 0.1	98.7 ± 0.1	95.7 ± 0.1
Avg Diff	0.0	0.0	+0.4	+9.2	+2.3	+0.2	+5.7	+2.8	+1.6	+0.7	+2.1

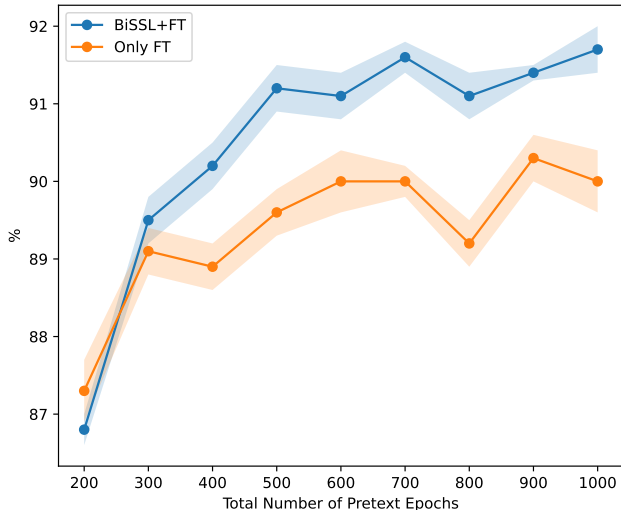


Figure 4. Top-5 test classification accuracies on the Flowers dataset for separate models pre-trained with SimCLR for different durations, comparing the conventional and BiSSL training pipelines. The corresponding top-1 accuracies are outlined in Figure 2.

are then forward-passed through the backbones. This procedure ensures that the batch normalization statistics are better suited to the downstream datasets, thereby providing a fairer comparisons of the learned representations.

For the dimensionality reduction and visualization of these latent features, the t-Distributed Stochastic Neighbor Embedding (t-SNE) (Cieslak et al., 2020) technique is employed. This method allows us to visually assess the clustering and separation of features in the latent space, providing qualitative insights into the semantic structure of the representations learned through BiSSL.

Figures 3 to 10 illustrate the outcomes of these visual inspections on a selection of the downstream datasets described in Section 4.1, highlighting the differences in feature representations between conventional pretext pre-training and BiSSL.

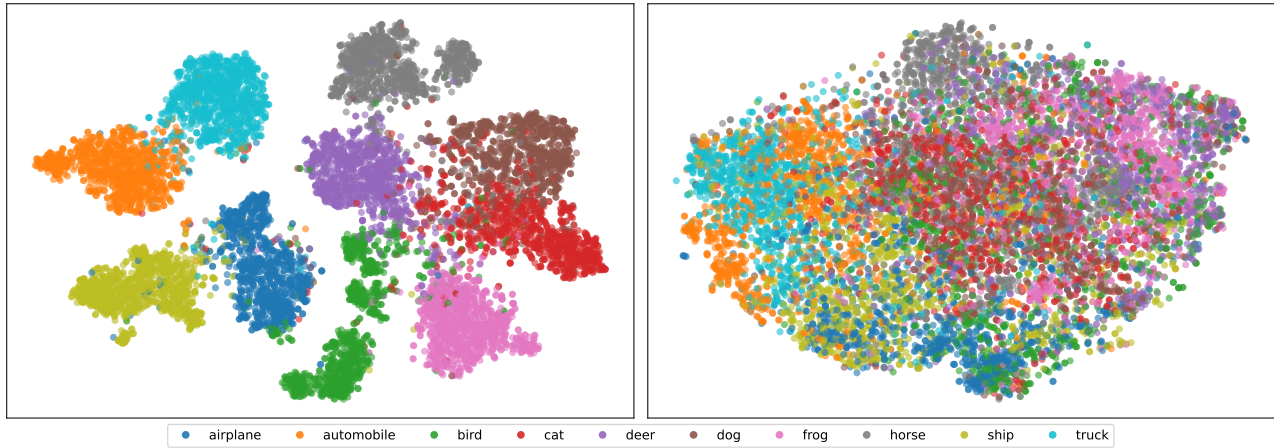


Figure 5. Features from lower-level backbones after applying BiSSL (left) or pretext pre-training (right) on the CIFAR10 dataset.

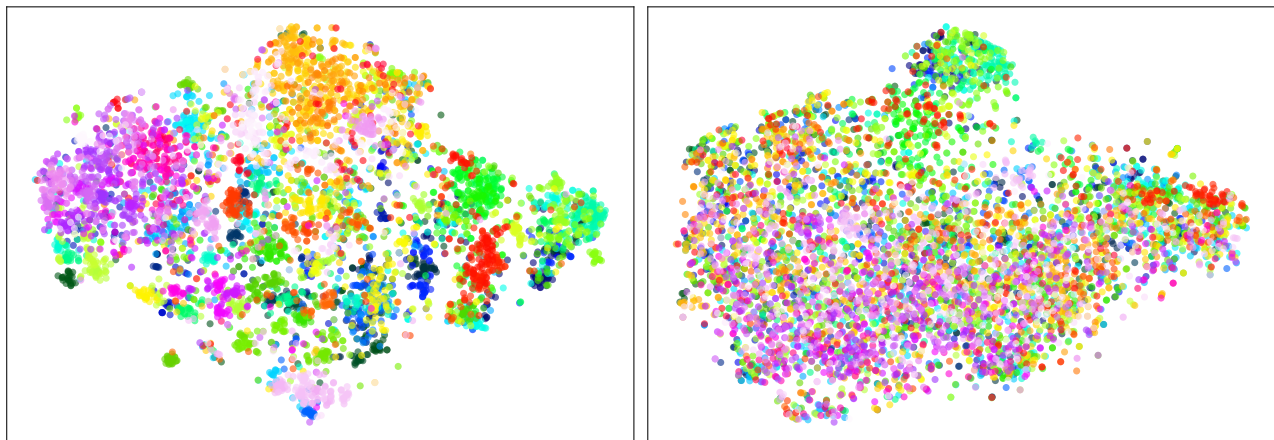


Figure 6. Features from lower-level backbones after applying BiSSL (left) or pretext pre-training (right) on the CUB200 dataset.

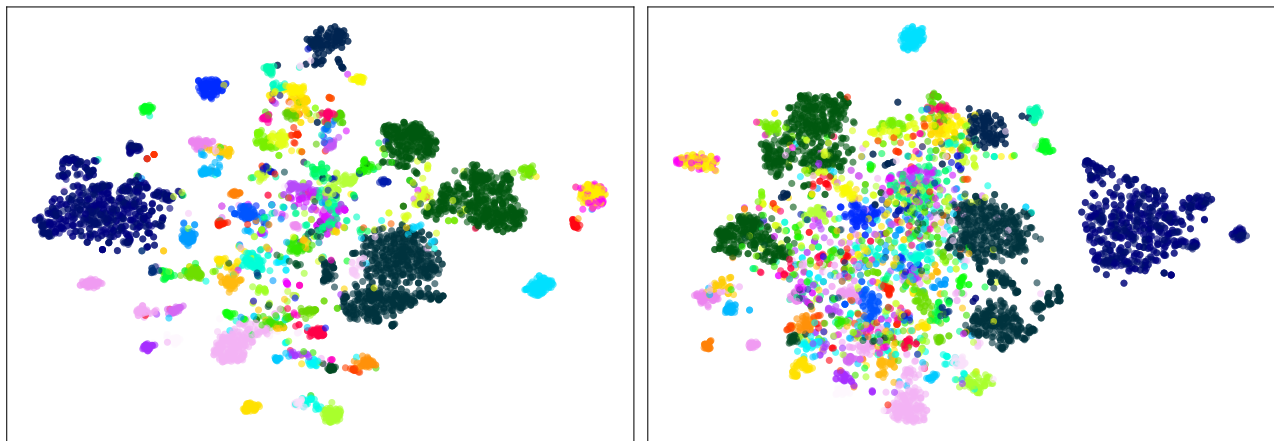


Figure 7. Features from lower-level backbones after applying BiSSL (left) or pretext pre-training (right) on the Caltech-101 dataset.

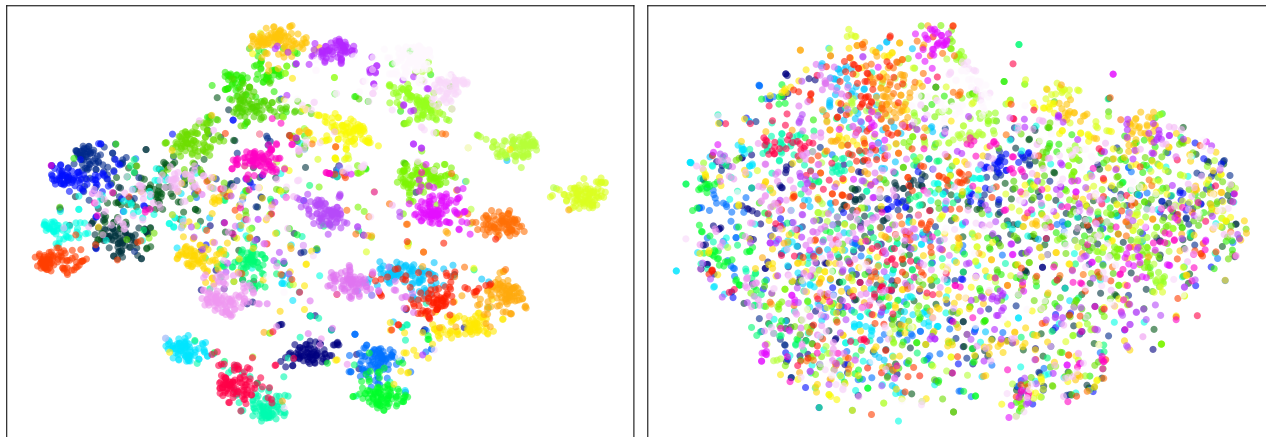


Figure 8. Features from lower-level backbones after applying BiSSL (left) or pretext pre-training (right) on the Pets dataset.

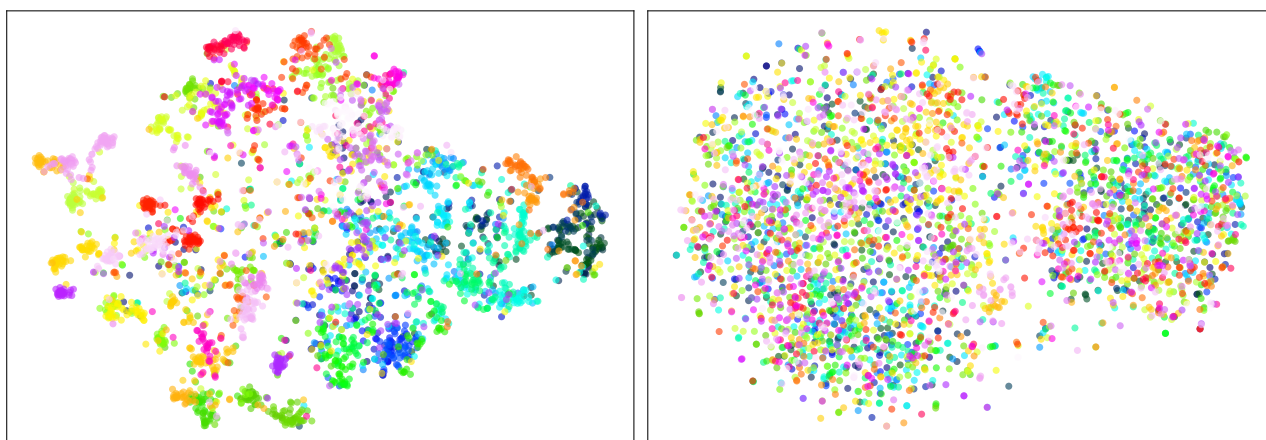


Figure 9. Features from lower-level backbones after applying BiSSL (left) or pretext pre-training (right) on the Aircrafts dataset.

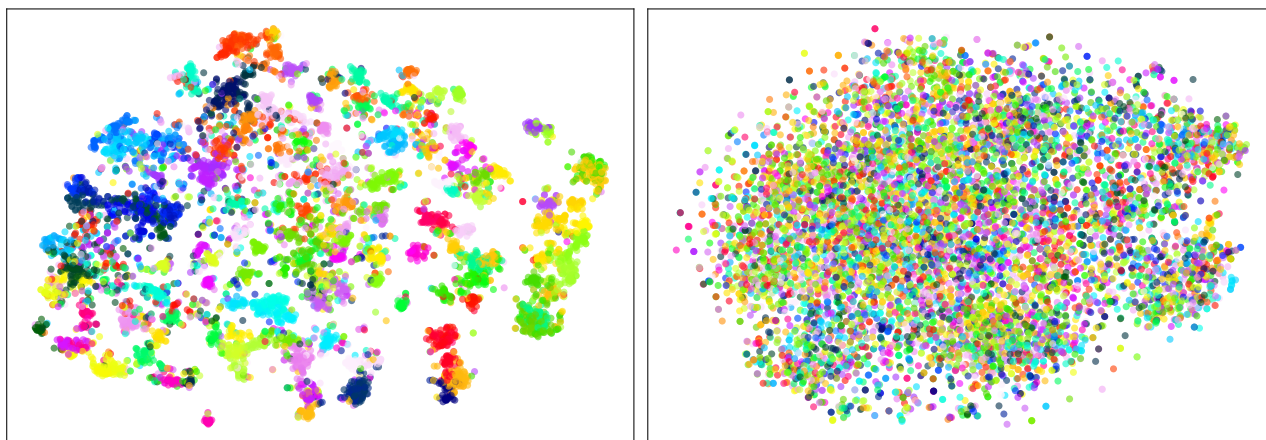


Figure 10. Features from lower-level backbones after applying BiSSL (left) or pretext pre-training (right) on the Cars dataset.